

Catalysis Science & Technology

Accepted Manuscript



This is an *Accepted Manuscript*, which has been through the Royal Society of Chemistry peer review process and has been accepted for publication.

Accepted Manuscripts are published online shortly after acceptance, before technical editing, formatting and proof reading. Using this free service, authors can make their results available to the community, in citable form, before we publish the edited article. We will replace this *Accepted Manuscript* with the edited and formatted *Advance Article* as soon as it is available.

You can find more information about *Accepted Manuscripts* in the [Information for Authors](#).

Please note that technical editing may introduce minor changes to the text and/or graphics, which may alter content. The journal's standard [Terms & Conditions](#) and the [Ethical guidelines](#) still apply. In no event shall the Royal Society of Chemistry be held responsible for any errors or omissions in this *Accepted Manuscript* or any consequences arising from the use of any information it contains.

Silica/MAO/(n-BuCp)₂ZrCl₂ Catalyst:**Effect of Support Dehydroxylation Temperature on the Grafting of
MAO and Ethylene Polymerization**

Muhammad Ahsan Bashir,^{a,c} Tom Vancompernelle,^b Régis M. Gauvin,^{b} Laurent Delevoye,^b Nicolas Merle,^a Vincent Monteil,^a Mostafa Taoufik,^a Timothy F. L. McKenna,^{a*} Christophe Boisson^{a*}*

^a Université de Lyon, Univ Lyon 1, CPE Lyon, CNRS, UMR 5265, C2P2 (Chemistry, Catalysis, Polymers & Processes), Bat 308F, 43 Bd du 11 Novembre 1918, 69616 Villeurbanne, France

^b UCCS (CNRS-UMR 8181), Université Lille Nord de France, USTL-ENSCL, 59652 Villeneuve d'Ascq, France

^c Dutch Polymer Institute (DPI), P.O. Box 902, 5600 AX Eindhoven, the Netherlands.

KEYWORDS: Silica dehydroxylation temperature, metallocene, methylaluminoxane, solid state NMR, ethylene polymerization

AUTHOR INFORMATION

Corresponding Authors

*E-mail: Christophe.boisson@univ-lyon1.fr

*E-mail: Timothy.mckenna@univ-lyon1.fr

*E-mail: regis.gauvin@ensc-lille.fr

Abstract

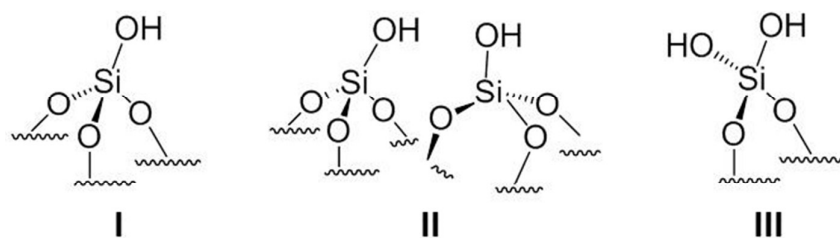
The current study aims to explore the link between the role of silica dehydroxylation temperature and the catalytic performance of an $(n\text{-BuCp})_2\text{ZrCl}_2$ metallocene precursor supported on silica impregnated with methylaluminoxane (MAO) in ethylene homopolymerization. Diffuse Reflectance Fourier Transform Infrared Spectroscopy (FT-IR-DRIFT) and Solid State Nuclear Magnetic Resonance (SS NMR) were used to study the generation of different Al species on the surface of silica impregnated with MAO after calcination at temperatures of 200°, 450° or 600°C. It was found that Si-CH₃ bonds can be formed when silica dehydroxylation temperature is $\geq 450^\circ\text{C}$, and that three different types of aluminum species are generated on silica surface, the nature of which does not change significantly with the silica dehydroxylation temperature. However, after grafting a metallocene precursor on the MAO-treated surfaces, an increase in the Zirconium loading, and in the intrinsic and average catalytic activities were observed with increasing silica dehydroxylation temperature. However, the molecular and physical properties of the high density polyethylene produced by using these catalysts are independent of the silica dehydroxylation temperature. These results indicated that the number of active sites on the surface of the catalyst increases with increasing dehydroxylation temperature, but the nature of the active sites does not.

Introduction

Amorphous silica is one of the most widely investigated and commonly used catalyst supports in the polyolefins industry. Metallocenes are anchored on pure, or methylaluminoxane (MAO)-modified amorphous silica to prepare supported (or heterogeneous) catalysts. Once supported, these catalysts can be employed in slurry or gas phase processes to produce different grades of polyolefins.¹ The benefits of using supported metallocenes (as opposed to homogenous catalysts) include the ease of their injection and removal of the final product in solid form, and the reduction of the risk of polymer film formation on the reactor walls which can in turn lead to poor heat removal from the reactor. A well-designed supported catalyst should offer good morphology control, high productivity, and ultimately, economic gains. One of the keys to obtaining these advantages is to ensure fine control of the surface chemistry of the support, and the procedure used to produce the MAO activated silica support (SMAO). Recent progress in deciphering MAO structure and its impact on the mechanism of metallocene activation leads us to believe that the cationic species $[AlMe_2]^+$ plays an important role in the activation process.^{2,3} It is important to investigate the impact of the grafting of MAO on silica on the performance of this activator.

It is well-known that geminal, vicinal and isolated hydroxyl groups (OH), known collectively as silanols, and water can be found on the surface of untreated silica particles (Scheme 1). Furthermore, it has also been well established in the open literature that the surface concentration of these OH groups can be reduced by heating the silica, leaving only isolated silanol and siloxane (Si-O-Si) bridges at temperatures above 500°C.⁴⁻¹⁰ On the other hand, it is difficult to know a priori what type and concentration of silanol groups are optimal in terms of activating a given metallocene precursor. Depending on the size and shape of the metallocene, one needs to minimize the steric hindrance to the incoming catalyst precursor or co-catalyst molecule, to prevent bimolecular deactivation, and promote the generation of the

active metallocenium cation, all of which contribute in determining the activity and performance of the catalyst. For example, $(n\text{-BuCp})_2\text{ZrCl}_2$ is one of the metallocenes that has found its application in industrial as well as academic research,¹¹⁻¹³ yet few studies have been carried out in order to understand the effect of silica dehydroxylation temperature on its activity.^{6,8,10,14} Since it has been shown^{1,14} different synthesis methods give different activities of the silica supported metallocenes, the most probable reason for this lack of clarity seems to be that different catalyst synthesis procedures were used in the previously cited studies, as discussed briefly in the next paragraph. It is therefore difficult to draw a clear conclusion on what, if any, relationship exists between the silica dehydroxylation temperature and the catalytic activity. In other words, whether or not a decrease in the concentration of OH groups on the silica surface helps to increase the activity of the supported catalyst.



Scheme 1. Schematic representation of Isolated (I), Vicinal (II) and Geminal (III) silanol groups on the surface of silica.

Santos et al.,⁶ analyzed the effect of silica dehydroxylation temperature on the metal loading on silica, catalytic activity in slurry ethylene polymerizations, the molecular weight distribution and crystallinity of the obtained polyethylenes. The catalysts were prepared by grafting $(n\text{-BuCp})_2\text{ZrCl}_2$ on Grace 948 silica dehydroxylated in the temperature range of 27 °C to 450 °C. MAO (10 wt% toluene solution) was added separately to the reactor in order to obtain Al/Zr molar ratio in the range of 100-5000, and the polymerizations were done at only

1 bar ethylene pressure. Using the same zirconocene, van Greiken et al.,¹⁰ studied the effect of silica dehydroxylation temperature (in the range of 200 to 600 °C) on the catalytic activity by grafting a pre-mixed solution of MAO (30wt% toluene solution) and $(n\text{-BuCp})_2\text{ZrCl}_2$ on the dehydroxylated silica in toluene slurry at room temperature for 3h. Another study dedicated to the effect of silica dehydroxylation temperature on the catalytic activity of $(n\text{-BuCp})_2\text{ZrCl}_2$ was reported by Atiqullah et al.,⁸ who calcined the commercial ES-70 silica in the temperature range of 250 to 800 °C. The calcined silica were functionalized by $n\text{-BuSnCl}_3$ at 130 °C before impregnation with MAO and grafting of the zirconocene at room temperature.

Given the diversity of the conditions used in these studies, it is difficult to identify a single silanol concentration which provides maximum catalytic activity for the silica supported $(n\text{-BuCp})_2\text{ZrCl}_2$ in ethylene homopolymerization at conditions of industrial relevance, and to understand the reason due to which silica dehydroxylation temperature affects the catalytic activity. Furthermore, keeping in mind the fact that MAO has a significant effect on the catalytic performance of supported $(n\text{-BuCp})_2\text{ZrCl}_2$, the effect of varying silanol concentration on the nature of Aluminium species generated after the interaction of MAO with silica cannot be understood based on the above mentioned studies. Other works related to the influence of silica dehydroxylation temperature on the catalytic activity of supported metallocenes in olefin polymerization focus catalysts different from $(n\text{-BuCp})_2\text{ZrCl}_2$ and therefore report different results.^{15,16}

The goal of the present study is to investigate the influence of silica dehydroxylation temperature on i) the type(s) of Aluminium specie(s) generated on the silica surface after impregnating MAO on silica dehydroxylated in the temperature range of 200 to 600 °C (i.e., by preparing SMAO) and ii) the catalytic performance of the active species generated on the surface of these SMAO samples after grafting the $(n\text{-BuCp})_2\text{ZrCl}_2$ metallocene in ethylene

homopolymerizations. In order to achieve this, an optimized incipient wetness method has been selected to make SMAO samples and the final supported catalysts.¹ The catalysts were then evaluated in both slurry and gas phase ethylene homopolymerizations at conditions of industrial relevance.

The benefit of using SMAO supported metallocene is twofold i.e., it allows one to study the interactions between hydroxyl groups of silica and the MAO molecule, and the leaching of the catalyst during polymerization is suppressed, thereby ensuring that the catalytic reaction takes place mainly on the silica surface (rather than in solution). In addition, Diffuse Reflectance Fourier Transform Infrared Spectroscopy (FT-IR-DRIFT) analysis of the SMAO and of the catalysts (SMAO-(*n*-BuCp)₂ZrCl₂) coupled with a Solid State Nuclear Magnetic Resonance (SS NMR) characterization of SMAO are reported. The results are used to provide unique information on the nature of chemical species formed on the surface of silica after impregnation of MAO which subsequently influences the catalytic activity of the resulting supported metallocene catalyst.

Experimental section

Materials

Grace 948 silica with a surface area of $290 \text{ m}^2 \text{ g}^{-1}$, average particle diameter of $58 \text{ }\mu\text{m}$ and a pore volume of 1.7 mL g^{-1} was used as the catalyst support. $(n\text{-BuCp})_2\text{ZrCl}_2$ was obtained from Sigma-Aldrich. Triethylaluminium (TEA) and triisobutylaluminium (TIBA) were used as received from SGS and Witco Corporation, respectively. The MAO solution 30 wt% in toluene used in this study was purchased from Albemarle with the following characteristics: 13.6 wt% Al, 5.24 wt% AlMe_3 , $\text{gas/Al} = 1.65$. n-heptane used in catalyst synthesis and as a diluent in slurry polymerizations was dried on 3 \AA molecular sieves.

Ethylene (purity 99.95%) was purchased from Air Liquide (Paris, France) and passed through three different purification columns before use: a first one filled with reduced BASF R3-16 catalyst (CuO on alumina), a second one filled with molecular sieves (13X, 3A, Sigma-Aldrich), and a last one filled with Selexsorb COS (Alcoa).

Drying of MAO

White powder of dried MAO was obtained by first evaporating toluene from 30 wt% MAO commercial solution. Subsequently, the powder was dried under a dynamic vacuum of 10^{-3} to 10^{-5} mbar for 4 h at $80 \text{ }^\circ\text{C}$. The dried MAO was then stored in a glove box.

Catalyst synthesis

For silica dehydroxylation, 3 g of Grace 948 silica were taken in a Schlenk tube and heated under dynamic vacuum of 10^{-3} to 10^{-5} mbar following the profiles shown in Figure S1. The profiles for 450°C and 600°C are similar except the maximum temperatures. For 200°C profile, silica was heated at 130°C for 1h in order to remove all the adsorbed water whereas for the other two profiles this was achieved by heating for 2 h at 200°C . A time of 4h was

given at maximum temperature under vacuum for all profiles. After dehydroxylation, silica was kept in the glove box.

The silica impregnated with MAO, named hereafter as SMAO, was prepared as follows. 2 g of dehydroxylated silica were placed in a three neck round bottom flask in the glove box under Argon. An amount of pure dry toluene equal to the pore volume of silica i.e., 1.7 ml g^{-1} was mixed with 3.5 ml of 30 wt% MAO solution in a separate vial at room temperature under argon and left for 30 min. This solution of MAO in toluene was then added to the silica drop-wise, which wetted the silica completely. The resulting thick slurry was heated at 80°C for 4h without any stirring under argon and the evaporating toluene was refluxed via a condenser. At the end of this process, the mixture was washed once with heptane, then dried under static vacuum at 80°C . Dried SMAO, a free flowing white powder, was stored in a glove box.

Supported metallocene catalysts were synthesized by adding 2 g of SMAO to a three necked round bottom flask and adding a 10 mL solution of $(n\text{-BuCp})_2\text{ZrCl}_2$ in toluene drop-wise at room temperature under argon in order to obtain a Al/Zr molar ratio of 150 in the final catalyst. The volume of toluene solution was just enough to completely fill the pores. The slurry was then heated for 1h at 50°C followed by one heptane wash and vacuum drying at 50°C for few hours. Finally a free flowing catalyst was obtained which was then stored in a glove box.

Polymerization procedure

Polymerization runs were carried out in a spherical laboratory scale 2.5 L semi-batch reactor which can be operated both in slurry and gas phases. The detailed reactor set-up has been described elsewhere.¹⁷ The reactor was conditioned for at least 1h at 80°C with a minimum of three argon-vacuum cycles, and then cooled down to the room temperature. For slurry

polymerizations, 500 mL of dry heptane containing 30 to 40 mg of catalyst and 1 mL of a 1 M solution of triethyl aluminium (TEA) or triisobutyl aluminium (TIBA) were added under argon into the reactor at room temperature. The reactor was then heated to the reaction temperature of 80°C under continuous stirring at 400 rpm. Ethylene was injected and maintained at a pressure of 8 bars once the desired reaction temperature was achieved. Consumption of ethylene was recorded by following the pressure drop in an ethylene cylinder equipped with a pressure gauge.

For gas phase polymerizations, 30 g of dry sodium chloride (NaCl) was used as a seed bed. The salt was dried twice at 400°C for 4 h under vacuum of 10^{-3} mbar in order to remove all the adsorbed water. In order to prepare the seed bed, 30 g of dried NaCl were mixed with 15 to 18 mg of catalyst in a 100 mL flask inside a glove box and then transferred into the reactor under argon pressure. 1 mL of 1 M solution of TIBA in n-heptane was then added into the reactor under argon flow at 70°C. Then reactor temperature was then raised to 80°C. Ethylene was injected into the reactor once the desired reaction temperature was achieved under continuous stirring at 400 rpm. The reactions were stopped by venting the gaseous ethylene through reactor exhaust and cooling the reactor to 20°C. The obtained polyethylene powder was then poured into a beaker of water where the salt was dissolved during overnight while stirring at room temperature.

Reaction time was 1 h for slurry polymerizations and 2 h for gas phase polymerizations.

Silica, SMAO and Catalyst Characterization

Al and Zr content of the final catalysts were measured using Inductively Coupled Plasma-Atomic Emission Spectroscopy (ICP-AES) at Mikroanalytisches Labor Pascher, Germany.

Diffuse Reflectance Fourier Transform Infrared spectroscopy (FT-IR-DRIFT) was used to characterise the as-received Grace 948 silica, the silica dehydroxylated at different

temperatures, and MAO impregnated silica (SMAO) prepared by using silica dehydroxylated at different temperatures and the final catalysts. A few milligrams of each sample were added to a DRIFT cell equipped with CaF₂ windows inside a glove box. For dried MAO, the sample was mixed with dry KBr (10wt%). IR spectra were recorded on a Nicolet 6700 FT-IR spectrometer. Typically, 64 scans were accumulated for each spectrum (resolution 4 cm⁻¹).

Solid-state NMR spectra were acquired on a Bruker Avance III 800 spectrometer (¹H: 800.13 MHz, ²⁷Al: 208.50 MHz). For ¹H experiments, the spinning frequency was 20 kHz, the recycle delay was 5 s and 128 scans were collected using a 90° pulse excitation of 2.25 μs. The ²⁷Al MAS NMR spectra at 18.8 T were acquired at a spinning frequency of 20 kHz, using central transition –selective Hahn echo sequence. The D-HMQC experiments were set up with a ²⁷Al spin echo selective to the central transition, with pulses of 8 and 16 μs, with ¹H π/2 pulse of 3.3 μs on either side of the ²⁷Al π pulse. The number of scans for each t1 increment was set to 1280. The dipolar recoupling scheme (SR4²₁) was applied for 600 μs.¹⁸ Two-dimensional (2D) ¹H-¹H Double Quantum Magic-Angle Spinning spectra were performed at 20 kHz spinning speed using the R12₂⁵ symmetry-based recoupling scheme¹⁹ applied for 133 μs at RF field strength of 65 kHz. The recycling delay was set to 2 s and 16 transients were added for each of the 100 t1 increments. The ²⁷Al MQMAS spectra were collected using the Z-filter sequence,²⁰ which consists of two hard pulses of 3.5 and 1.3 μs at an RF field of 90 kHz, for triple-quantum excitation and reconversion, respectively, followed by a soft pulse of 6 μs at an RF field of 15 kHz. The t1 step was set to the MAS period. Chemical shifts were given in ppm with respect to TMS as external reference for ¹H NMR, and to Al(H₂O)₆³⁺ for ²⁷Al NMR. The samples analyzed by NMR were: dried MAO, SMAO-

200°C, SMAO-450°C and SMAO-600°C. The samples were prepared under strictly inert conditions in an argon-filled glovebox by packing into ZrO₂ rotors closed with Kel-F caps.

Polymer Characterization

High Temperature Size Exclusion Chromatography (HT-SEC) analyses were performed using a Viscotek system (from Malvern Instruments) equipped with three columns (PLgel Olexis 300 mm x 7 mm I. D. from Agilent Technologies). 200 µL of sample solutions with a concentration of 5 mg mL⁻¹ were eluted in 1,2,4-trichlorobenzene using a flow rate of 1 mL min⁻¹ at 150°C. The mobile phase was stabilized with 2,6-di(tert-butyl)-4-methylphenol (200 mg L⁻¹). Online detection was performed with a differential refractive index detector and a dual light scattering detector (LALS and RALS) for absolute molar mass measurement. The OmniSEC 5.02 software was used for calculations.

Thermal characterizations were performed with a differential scanning calorimetry, Mettler Toledo DSC 1, equipped with an auto-sampler and a 120 thermocouple sensor. The temperature and the heat flow of the equipment were calibrated with an indium standard. All samples were accurately weighed (between 5 to 10 mg) and sealed in aluminium pans. They were heated from -20 °C to 180 °C at 10 °C.min⁻¹ with an empty aluminium pan as reference. Two successive heating and cooling were performed and only the second run was considered. Dry nitrogen with a flow rate set at 50 mL.min⁻¹ was used as the purge gas. The melting temperature (T_m) was measured at the top of the endothermic peak. The STAR^c thermal analysis software is used to calculate the melting temperature and the crystallinity (χ) of the polymers: $\chi = \Delta H_f / \Delta H_{f0}$ where ΔH_f (J.g⁻¹) is the melting heat of the sample and ΔH_{f0} (= 293 J.g⁻¹) the melting heat of a 100 % crystalline polyethylene.²¹

Results and Discussion

The manner in which supported catalysts (metallocene or other) are prepared can eventually have an impact on the quantity and nature of the active species, and if so, this can influence the rate of polymerization, as well as the molecular and physical properties of the final polymer product. As we mentioned above, various routes for the preparation of silica-supported metallocenes have been proposed in the literature, and each synthesis procedure has specific advantages.^{6,8,10,14,22,23} Supporting MAO on dehydroxylated silica before grafting the metallocene is one of the most common methods discussed in the open literature. However, the role of the dehydroxylation temperature of silica on the grafting of MAO, which in turn impacts the performance of the catalyst, has not been directly studied or clearly explained.

In the present work three SMAO/(n-BuCp)₂ZrCl₂ catalysts were prepared using the Grace 948 silica treated at 200°C, 450°C or 600°C. The dehydroxylation of silica was followed by the impregnation of a toluene solution of 30 wt% MAO (Albemarle) for 4 h at 80°C. The chemical formula of the MAO can be determined from the analysis provided by the supplier (see experimental part). In agreement with the work of Imhoff et al.,²⁴ the formula of MAO can be represented as (Al(CH₃)_{1.42}O_{0.79})_n and free trimethylaluminium (TMA, representing 14.4% of Al). The final product of this step was a white free flowing powder named as SMAO-200°C, SMAO-450°C or SMAO-600°C depending upon the silica dehydroxylation temperature used. The activation of (n-BuCp)₂ZrCl₂ on each SMAO i.e., SMAO-200°C, SMAO-450°C and SMAO-600°C was carried out by first mixing the toluene solution of metallocene with SMAO followed by heating at 50°C for 1h under Argon without any stirring. One wash of heptane was applied at 50°C immediately after the end of the reaction, and the mixture was then dried under vacuum at 50°C. The final catalyst was a free

flowing light green powder, which will be referred, hereafter, as n-BuCp-200°C, n-BuCp-450°C and n-BuCp-600°C depending upon the silica dehydroxylation temperature used.

The elemental analysis of these catalysts by ICP-AES is presented in **Table 1**. The aluminium content of the final catalysts decreased with the increase of the silica dehydroxylation temperature. The Al/Zr molar ratio was close to the targeted ratio of 150 based on a full impregnation of the MAO and of the metallocene complex when the silica was thermally treated at 450 and 600°C. Surprisingly, the Zr content for the n-BuCp-200°C catalysts was lower than expected. It can be assumed that the supported activator SMAO-200°C displays lower number of activating sites, leading to a lower grafting of the metallocene. We can thus suppose that the nature of the silanol groups on silica support, which is controlled by the thermal treatment of the silica, impacts the structure of the supported MAO and consequently its ability to react with a metallocene precursor. DRIFT and SS-NMR analyses of SMAO were performed for characterizing the SMAO and provided some information regarding the difference of reactivity between MAO and the Grace 948 silica treated, respectively, at 200°C, 450°C or 600°C.

Table 1. Elemental analysis of the supported catalysts prepared by using different silica dehydroxylation temperatures.

Silica	Al	Zr	Al	Zr	Al/Zr
T(°C)	(wt%)	(wt%)	moles	moles	
200	16.24	0.11	6.02E-03	1.21E-05	499
450	13.45	0.29	4.99E-03	3.18E-05	157
600	11.40	0.26	4.23E-03	2.85E-05	148

DRIFT Analysis of Silica, dried MAO, SMAO and Supported Metallocene Catalysts

Silica surface hydroxyl (OH) groups are characterized as isolated silanol (**scheme 1, I**), vicinal silanol (**scheme 1, II**) and geminal silanol (**scheme 1, III**). These silanol groups act as fixation sites for the cocatalysts or metallocenes depending upon the method of catalyst synthesis, and their concentrations decrease with an increase in silica dehydroxylation temperature. DRIFT is an essential analytical tool for analysing different type of chemical species present on silica surface and it has been used extensively to characterize different species present or generated on the silica surface before and after dehydroxylation, impregnation with MAO and metallocene grafting.^{4-7,25,26} The DRIFT spectra of 600 °C dehydroxylated Grace 948 silica, SMAO-600°C and n-BuCp-600°C are compared in Figure 1 (See also Figures S2 and S3 in supporting information for silica treated at 200°C and 450°C, respectively). In addition to isolated silanol groups (peak at 3736 cm⁻¹), it can be observed that vicinal OH groups (peak at 3661 cm⁻¹ and 3536 cm⁻¹) are also present after heat treatment at 200°C,⁶ whereas only isolated silanol groups remain on the silica after treatment at 450°C and 600°C. Broad bands at 1870 cm⁻¹ and 1632 cm⁻¹ are overtones and result from combination of intense Si-O fundamental modes. These results are in good agreement with available literature data.⁴⁻⁷

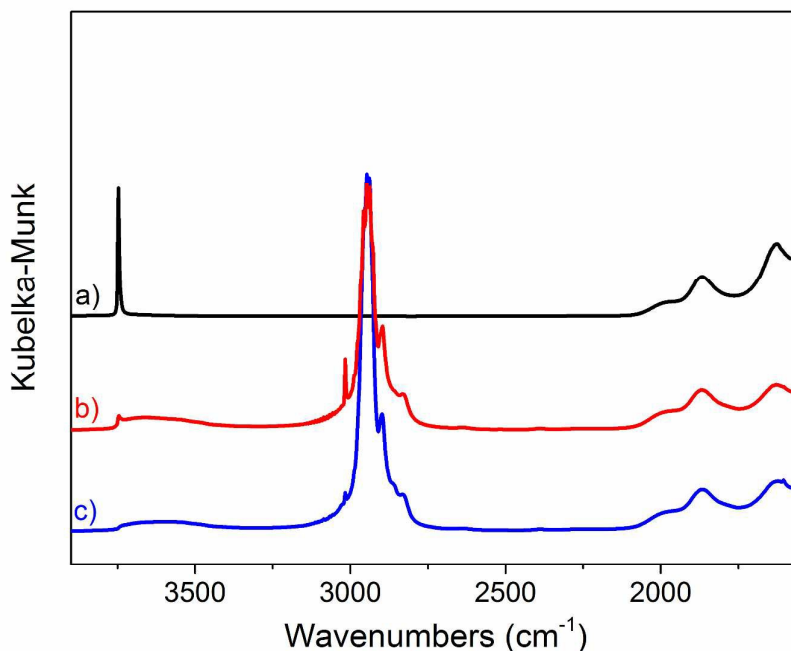


Figure 1. DRIFT spectra of silica-600°C (a), after reaction of MAO (SMAO-600°C) (b), after activation of $(n\text{-BuCp})_2\text{ZrCl}_2$ (n-BuCp-600°C) (c).

After impregnation of each silica with MAO, new peaks appear, especially in the range of 3100 to 2700 cm^{-1} due to the reaction of MAO with different silanol groups present on silica. Since, MAO is a mixture of oligomeric MAO and TMA,^{5,27} it has been suggested that, depending on the dehydroxylation temperature, silanol (Si-OH) or siloxane (Si-O-Si) groups react with TMA, whereas MAO is physically adsorbed on the surface.^{5,6,9} The reaction of TMA with OH groups generate -Si-O-Al(CH₃) species, whereas, -Si-CH₃ moieties are produced by the reaction of Al-CH₃ species with Si-O-Si siloxane groups.^{5,27} For SMAO-200°C and SMAO-450°C, isolated silanols are totally consumed by reaction with MAO in contrast to SMAO-600°C, as indicated by a small band at 3745 cm^{-1} in Figure 1 characteristic of isolated silanols. This peak totally disappeared after metallocene grafting. Hydrogen bonded OH groups can be observed in all the SMAO samples in the range of 3680 to 3660 cm^{-1} .

Methyl groups of MAO can be observed in the region of 3000 to 2800 cm^{-1} with v_a and v_s of the terminal methyl groups in the range of 3050-2018 cm^{-1} and 2950-2750 cm^{-1} .^{4,5} In case of SMAO-450°C and SMAO-600°C, very similar peaks can be observed at 2957, 2947, 2940 and 2900 cm^{-1} . These peaks can be attributed to the stretching vibrations of methyl groups in Al-CH₃ species or Si-CH₃ species. Distinction between the two species (i.e., Al-CH₃ or Si-CH₃) based on DRIFT spectra is difficult because the stretching vibrations of methyl groups in both the species are very similar,^{5,27} however both Bianchini et al.⁴ and Panchenko et al.⁵ attributed the peak at 2960 cm^{-1} to the presence of Si-CH₃ species. The DRIFT spectra of SMAO samples show the presence of this peak in SMAO-450°C and SMAO-600°C at 2957 cm^{-1} , whereas, no such peak is present in the SMAO-200°C sample. This is due to the fact that reactive siloxane bonds (Si-O-Si) are formed only at higher dehydroxylation temperatures. The DRIFT spectrum of SMAO-200°C (i.e., Figure S2) showed peaks at 2949 and 2900 cm^{-1} due to the stretching vibrations of methyl groups in Al-CH₃ species.^{4,5} In addition, the DRIFT spectrum of dried MAO (Figure S4) showed peaks at 2947, 2937 and 2895 cm^{-1} for the stretching vibrations of methyl groups in Al-CH₃ species. This analysis confirms the assignment of peaks observed in the same region for SMAO. In summary DRIFT analyses of dehydroxylated silica, SMAO and supported metallocene showed that the nature of surface species is influenced by the reactivity of silanol and siloxane moieties, which depends on the thermal treatment of silica.

DRIFT spectra of the final supported catalysts (i.e., after grafting the metallocene on SMAO) are also shown Figure 1, Figure S2 and Figure S3. It is important to mention that characteristic absorption peaks of the aromatic and alkyl groups present in the (n-BuCp)₂ZrCl₂ molecule appear in the same region as that of MAO molecule i.e., 3100-2800 cm^{-1} (C-H stretching) and 1500-1300 cm^{-1} (methyl and methylene deformation modes).⁶ It is therefore difficult to differentiate between the DRIFT peaks coming from metallocene, MAO

and toluene molecules. However, the peak at 1602 cm^{-1} can be attributed to -C=C- stretching of the Cp ring, whereas, the one at 1494 cm^{-1} can be attributed to bending vibrations $\delta(\text{CH}_3)$ of the butyl substituent of the Cp ligand^{25,28} and appears in the DRIFT spectra of all the final supported catalysts only. The stretching vibrations at 3016 cm^{-1} have been attributed to the Cp ring by Bianchini et al.⁴ This peak was also observed in our spectra. However, it should be noted that residual toluene shows the same vibration (see SMAO spectra in Figure 1, Figure S2 and Figure S3).

Solid State NMR Analysis of dried MAO and SMAO samples

Liquid-state NMR studies on MAO and aluminoxanes have been previously reported in the literature.²⁹⁻³¹ In particular, given the possibility to determine the coordination number of aluminum alkyl from their chemical shift, ^{27}Al should be the most adequate tool to determine the structural features with MAO.^{32,33} However, since ^{27}Al is a quadrupolar nucleus ($S=5/2$), the broad line width encountered in non-highly symmetrical environments prevents any detailed analysis. On the other hand, solid state NMR provides access to additional spectroscopic parameters other than chemical shift. Namely, it is possible to determine quadrupolar coupling constants that are characteristic for given structural types. One can also benefit from high resolution techniques such as MQMAS to disentangle complex 1D spectra (*vide infra*). Indeed, a few studies on MAO and molecular models have been performed, with mixed conclusions regarding the actual MAO structure.^{34,35} It is therefore of interest to perform more detailed studies involving state of the art NMR methodology focused on structural investigations on MAO and to its grafting on silica. In the present study, we used high field NMR, combined with a high resolution method MQMAS for quadrupolar nuclei, as well as homo- and heteronuclear correlations to determine the main features of MAO and its silica-supported version along with the grafting reaction pathways. It is necessary to

account for the fact that we will be studying materials (dried MAO and SMAO) that have been subjected to vacuum treatment. Thus in the case of dried MAO, its composition differs from that of commercial MAO solutions since AlMe_3 (either free or bound) is present in solution but the vacuum treatment causes AlMe_3 elimination from the product (Figure S5).

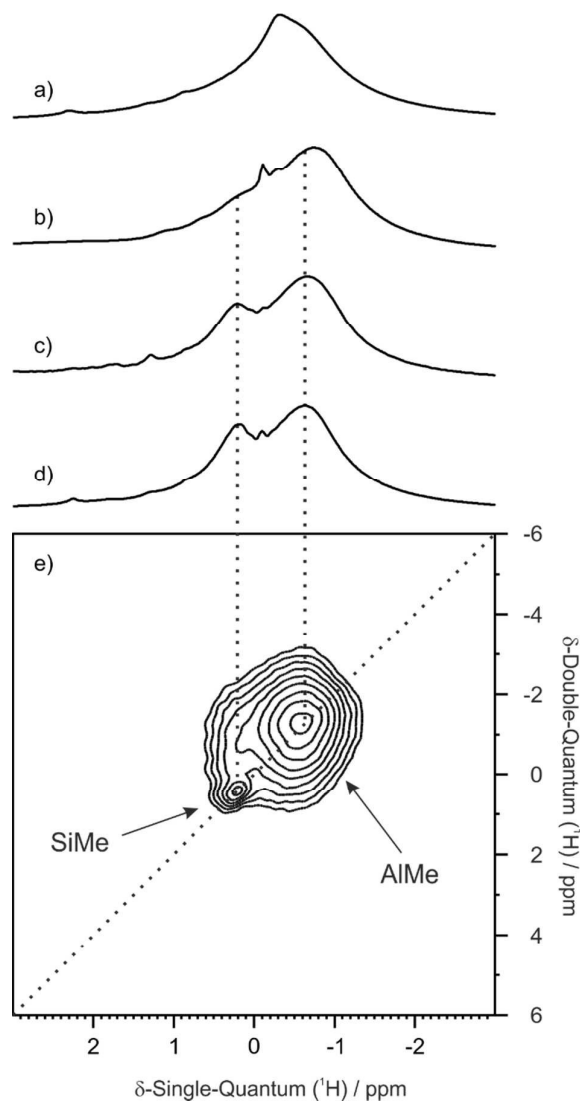
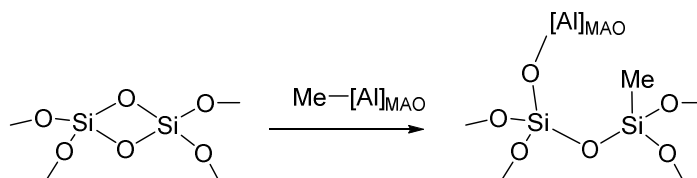


Figure 2. ^1H MAS NMR spectra of a) dried MAO, b) SMAO-200°C, c) SMAO-450°C and d) SMAO-600°C; e) ^1H - ^1H DQ MAS NMR spectrum of SMAO-600°C (18.8 T, spinning speed 20 kHz)

^1H MAS NMR spectra of dried MAO and supported MAO (SMAO-200°C, SMAO-450°C and SMAO-600°C) feature signals expected for Al-Me groups at a chemical shift (CS) of about -0.7 ppm (Figure 2a-d). A slight shift is observed in the position of the Al-Me signal upon grafting, from -0.4 ppm in dried MAO to about -0.7 ppm in the supported MAOs. Furthermore, when comparing spectra of SMAO-200°C and SMAO-600°C, one notices the increase of the 0.2 ppm signal assigned to Si-Me protons. This is in line with infrared studies described above. These groups arise from reaction of Al-Me with strained siloxane bridges, the proportion of which increases with silica dehydroxylation temperature (Scheme 2).

Proximities between protons within a solid can be determined using ^1H - ^1H Two-Dimensional (2D) Double-Quantum MAS NMR spectroscopy (DQ MAS), which relies on homonuclear dipolar recoupling methods.³⁶ The DQ MAS spectrum of SMAO-600°C (Figure 2e) shows that the Si-Me groups are close to some of the Al-Me moieties, as expected from the postulated reaction mechanism. This is highly reminiscent of the surface chemistry of AlMe_3 , where similar spectra are obtained (See Figure S6 in Supporting Information for comparison).^{37,38} This demonstrates that grafting of MAO occurs not only via Al-Me protonolysis, but also from Si-O-Si opening, which results in spatially close Si-Me and Al-Me groups (Scheme 2).



Scheme 2. Reaction of MAO with strained siloxanes

A further confirmation of proton signal assignment was brought by the ^1H - ^{27}Al D-HMQC spectrum.³⁹ This technique probes the spatial proximity of heteronuclear pairs, within a given

sphere radius. Using a short recoupling delay thus provides selective information on close spin pairs (below 4 to 5 Å). In the case of SMAO-600°C, the observed correlation with the ^{27}Al dimension (Figure 3) only concerns the -0.7 ppm ^1H signal, which confirms its assignment to Al-CH₃ group. Accordingly, no cross-peak is observed for the Si-Me site.

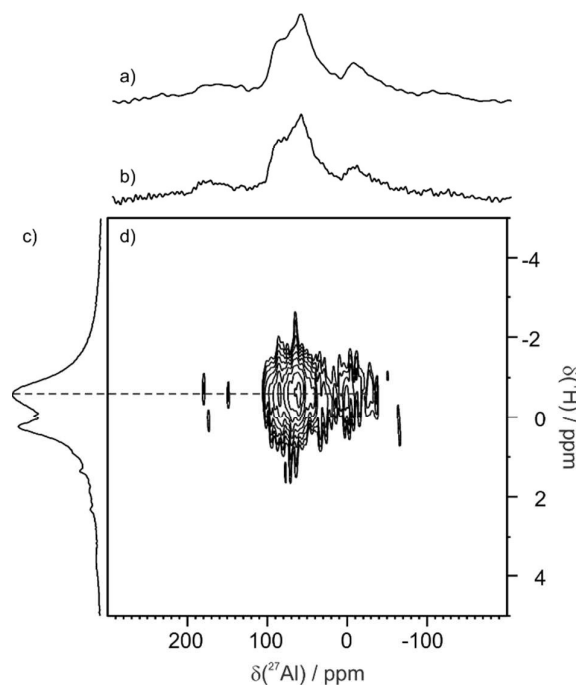


Figure 3. SMAO-600°C: a) ^{27}Al Hahn-echo, b) ^1H -filtered ^{27}Al D-HMQC, c) ^1H and d) 2D ^1H - ^{27}Al D-HMQC MAS NMR spectra (18.8 T, spinning speed 20 kHz)

The ^{27}Al Hahn echo MAS NMR spectra of dried MAO and supported MAO (Figure 4a-c) are composed of a broad resonance as a consequence of a large second-order quadrupolar interaction, not averaged under MAS conditions. In an initial stage, the spectra look similar, with a featureless signal [20-110 ppm], most probably resulting from the overlapping of several Al sites. The observed CS values are in line with those reported by Talsi²⁹, of about 110 ppm. In order to get a more precise insight into the dried MAO structure, we resorted to the 2D high resolution method MQ MAS.⁴⁰

The spectrum of the molecular sample of dried MAO has a good signal-to-noise ratio, but is rather complex, featuring peculiar line shapes due to large quadrupolar coupling associated with significant chemical shift anisotropy. This combination leads to a large number of highly distorted spinning side bands in the isotropic dimension ($\delta_1(^{27}\text{Al})$). This is reported in the literature for extreme cases such as ^{93}Nb MQ MAS NMR spectra of specific inorganic materials.^{41,42} Remarkably, in the present case, the distortion is such that it can result in the quasi-negligible intensity of the isotropic signal, with maximized intensity in the spinning side bands. The position of the isotropic signals was unambiguously determined by recording the MQ MAS spectrum at 2 different spinning speed (**Figure S7**). Thus, three main sites emerge from the high resolution spectrum: a) the major site (site A, **Figure 4**) features a chemical shift of 100 ppm, with a large quadrupolar coupling, of about 18 MHz (calculated from the position and width of the isotropic signal in the 2D spectrum);⁴³ b) a second site of lesser intensity (site B, **Figure 4**) resonates at 119 ppm, with also quadrupolar coupling above 18.5 MHz, similar to that of site A; c) a third site appears as a minor component at 69 ppm, with a broadening dominated by chemical shift distribution, and no apparent quadrupolar broadening (Site C, **Figure 4**). These parameters have been used successfully to simulate the CS lines on the MQ MAS spectrum (**Figure S8**). The reader's attention is drawn to the fact that in the case of spectra featuring quadrupolar lineshapes (as in the present cases), the isotropic chemical shift is not located in the center of the central transition signal, but on its lower frequency end.

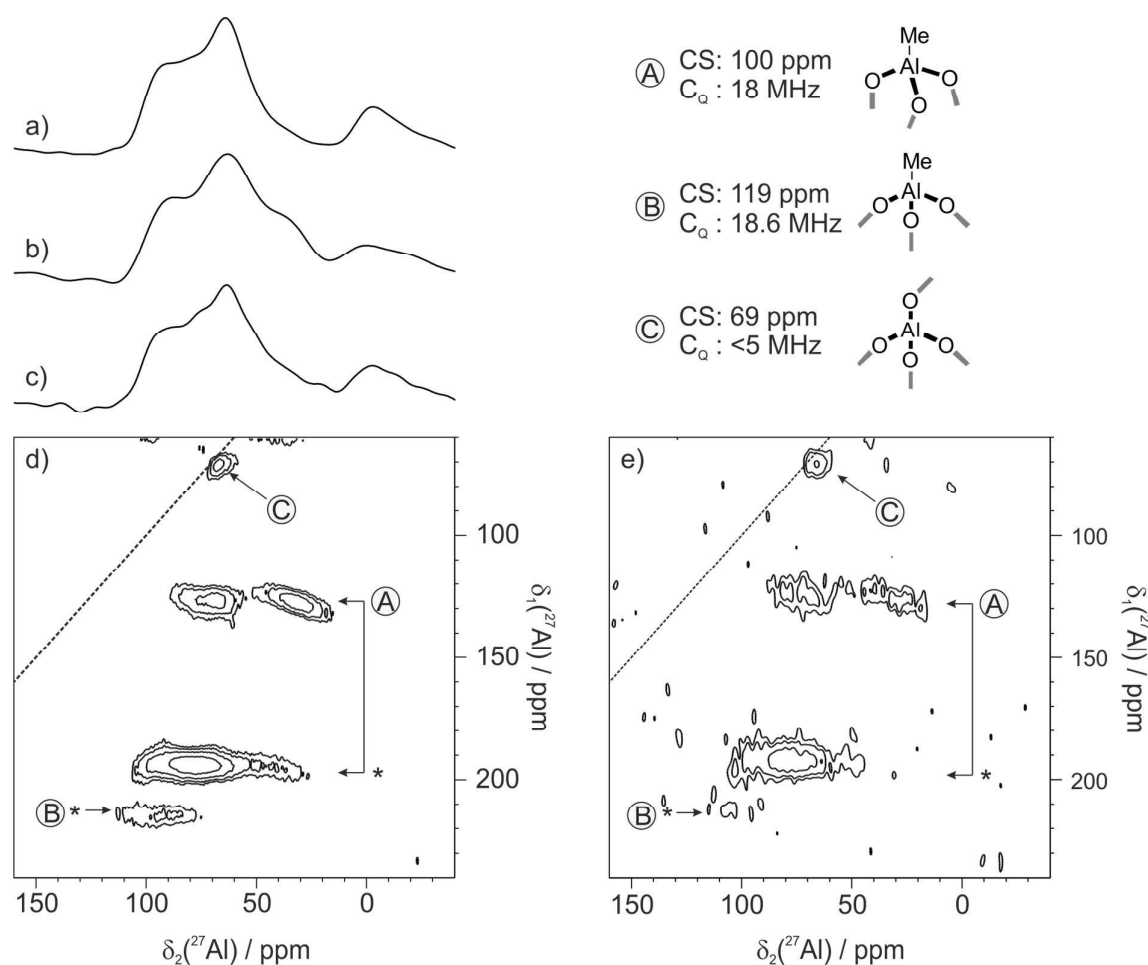


Figure 4. ^{27}Al Hahn Echo MAS spectrum of a) MAO, b) SMAO-200°C and c) SMAO-600°C, and ^{27}Al MQ MAS spectrum of d) MAO and e) SMAO-600°C (18.8 T, spinning speed 20 kHz); On spectrum d), the B species is evidenced by its rotation band at 215 ppm in the isotropic dimension, while the chemical shift band expected at 146 ppm is not observed due large anisotropic interactions associated with inhomogeneous MQ excitation conditions. Asterisks designate spinning side bands.

Thus, sites A and B feature rather similar chemical shift and quadrupolar coupling constant. The well-admitted main structural type within MAO is tetracoordinated $\text{Al}(\text{Me})\text{O}_3$. Molecular species with similar aluminum coordination spheres indeed give rise to CS in the 120-80 ppm range, which is in agreement with both observed values for A and B.^{30,44} The quadrupolar coupling constant is in the same range to that of MAO-related molecular species (where $\text{Al}(\text{Me})\text{O}_3$ display a C_Q value of 17.5 MHz³⁵) and of electronically comparable surface

monohydride on tetra-coordinated aluminum ($\text{Al}(\text{H})(\text{O})_3$) which features a C_Q value of about 15 MHz.⁴⁵ However, the rather well-separated lines for A and B in the MQ MAS and the lack of CS and C_Q distribution are indicative of two slightly but definitively distinct types of environments. Interestingly, the IFPEN theory group recently studied the structure of “pure” MAO cages, composed of $[\text{AlOMe}]_n$ units (with a 1:1 Al:Me ratio) arranged in either square or hexagonal faces, and computed the corresponding ^1H and ^{27}Al NMR chemical shifts.⁴⁶ They correlated the local environment of aluminum atoms in terms of nature of edge-sharing faces with ^{27}Al chemical shift. Based on this, we propose that site A (CS of about 100 ppm) is on the edge of 1 square and 2 hexagonal faces (calculated range: 103-109 ppm) and that site B (CS of about 119 ppm) is on the edge of 2 square and 1 hexagonal faces (calculated range: 111-120 ppm). This is depicted in **Figure 5**, which features as an example a cage structure involving 8 Al atoms. This is the first experimental evidence of the topology and structure of MAO-cages that have been postulated by DFT calculations.

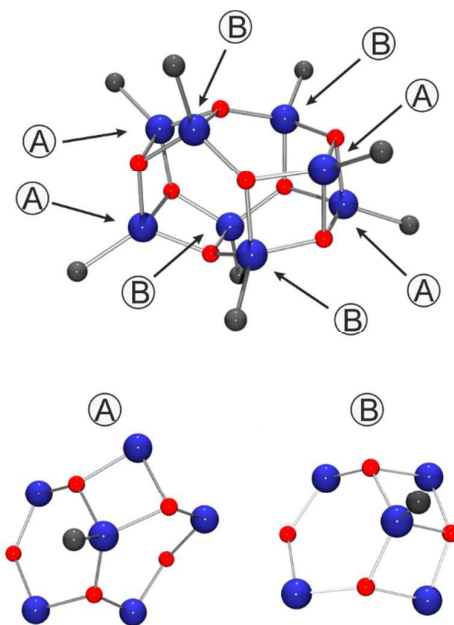


Figure 5. Example of $[(\text{AlMeO})_8]$ MAO-cage and the two A and B structures

Regarding site C, the low CS and C_Q values plead for a purely oxygenated coordination sphere, of the $Al(O)_4$ type.⁴⁷ Most specifically, the low C_Q (less than 5 MHz) rules out the hypothesis of $AlMeO_3$ sites on the edge of 3 hexagonal faces (calculated CS of 90 ppm). The low quantity of these sites may be an indication that they result from decomposition by hydrolysis or oxidation, although one cannot rule out that they are “buried” aluminum centers from larger structures within MAO.

Unfortunately, unambiguous determination of the proportions of these sites (and thus assessment of the average size of the oligomers based on DFT-calculated models) is out of reach, due to inhomogeneous site excitation for MQ MAS, to strong line shape overlapping of 1D spectra and to the occurrence of spectral components with fairly similar features (CS and C_Q). Furthermore, due to intrinsic NMR limitations, we cannot rule out the presence of aluminum centers featuring higher C_Q , as was proposed in several MAO models,^{34,35} or observed for silica-supported aluminum alkyls.⁴⁸ This means that bis- or tris-alkyl species such as $[Al(O)_nMe_m]$ ($n,m= 2$ or 3) that have been postulated in the literature may have escaped detection under our experimental conditions, and that we may not be observing all the aluminum centers present in the dried MAO sample. In particular, we did not observe oxygen-bound TMA in the above described spectra. This is a species postulated in the MAO structure that would give rise to signals in the 185-170 ppm range.^{32,49}

These elements can help to determine a range of possible structure with various nuclearity for the dried MAO. Indeed, in reference 45, the most stable $(AlOMe)_n$ structures have been determined by theoretical calculations. It appears that for value ‘n’ above 13, the number of hexagonal faces increases, while the number of square faces is constant. Thus, from thereon, the quantity of Al sitting on 3 hexagonal faces increases constantly with the nuclearity of the cages. Such Al centers give rise to an NMR signal expected at 90 ppm, which is not observed in the present case. On the other hand, below $n=12$, the proportion of such sites is

low (only 2 out of 10 and 2 out of 11 respectively for $(\text{AlOMe})_{10}$ and $(\text{AlOMe})_{11}$), below the detection limit of MQ MAS. Along the same line, the 'n' values less than 6 can be excluded based on high proportion of square faces. Thus, we propose that the nuclearity of the $(\text{AlOMe})_n$ is most probably between 6 and 12. This is much lower than reported values.⁵⁰ This discrepancy may be due to the thermal treatment of MAO upon its drying that affects the size of the cage. On the other hand, one can also propose that as NMR is sensitive to local parameters, as it gives evidence for low nuclearity, the larger MAO sizes determined in solution would be the result of aggregates formation by clustering of smaller entities.

The MQ MAS NMR spectrum of SMAO-600°C was recorded (**Figure 4e**). It features overall similar signals to that of dried MAO described above. This indicates that the structures present in the dried MAO are found in this material, obtained from reaction of MAO solution with silica followed by mild (80°C) thermal treatment under vacuum. In spite of the low signal-to-noise ratio due to the low Al concentration in the silica-supported sample, it appears that the B sites are preferentially consumed upon grafting (see **Figure S9** for the comparison of the isotropic projections of dried MAO and SMAO-600°C). However, further discussion is not possible at this stage.

In conclusion, both DRIFT and SS-NMR analysis of SMAO highlighted that the concentration and the nature of silanol and siloxane groups impact the reaction of MAO with silica. The analysis of SMAO obtained from silica thermally treated at elevated temperature (450-600 °C) showed the presence of Si-Me groups formed by opening of strained siloxane moieties. Thus, for silica treated at 200 °C the MAO reacts only with the silanol while for silica treated at higher temperature the MAO reacts first with the silanol and subsequently the surface Al-Me function opens siloxane moieties leading possibly to the formation of vicinal Si-CH₃ sites. We can reasonably assume that the way the MAO reacts with silica impacts the structure of the activator, and thus the number of activating sites leading to different Zr

content after impregnation of the metallocene precursor (see **Table 1**). Another important issue concerns the actual nature of the MAO compound that reacts with the silica surface. Indeed, MAO solution consists of a mixture of polymeric MAO fraction $(\text{Al}(\text{CH}_3)_{1.42}\text{O}_{0.79})_n$ and free trimethylaluminium (TMA). It is well accepted that the TMA reacts preferentially with silica due to its smaller size and its higher reactivity. However, we cannot rule out direct reaction of polymeric MAO, especially with silica treated at low temperature (200°C) where a sub-stoichiometric amount of TMA (related to Si-OH concentration) was introduced. The nature of the aluminum species that reacts can obviously impact the number of activating site on SMAO. It appears that a thermal treatment of silica at elevated temperature leading to a lower concentration of silanol group (isolated silanol) favored the grafting of the metallocene $(n\text{-BuCp})_2\text{ZrCl}_2$. However, further discussion is not possible at this stage. Another observation is the fact that the structure of SMAO is close to that of dried MAO, namely consisting of cage structures.

Catalyst Evaluation

This part of the work describes the impact of silica thermal treatment on the catalytic efficiency of the SMAO/ $(n\text{-BuCp})_2\text{ZrCl}_2$ in, both, slurry and gas phase homopolymerizations. The effect of the silica dehydroxylation temperature on the catalytic activity was evaluated at 80°C in slurry and gas phase ethylene homopolymerization at pressures of 8 and 11 bar of ethylene, respectively. Two different alkylaluminium compounds i.e., TEA and TIBA were used to see how the catalysts behave in the presence of different scavengers, and to confirm that the silica dehydroxylation temperature has a similar effect on the catalytic activity independently of the specific alkylaluminium or scavenger. It should be noted that the

concentration of both the scavengers was 2 mmol.L⁻¹ for the slurry phase reactions and 1 mmol of alkylaluminium was injected in a 2.5 L reactor for the gas phase polymerizations.

Figures 6 and 7 show that the catalytic activity in slurry phase reactions increased with increasing silica dehydroxylation temperature for both alkylaluminiums. However, the rate profiles obtained with TEA and TIBA show some differences. Stable rate profiles with slow activation and almost no decay in catalytic activity over a polymerization time of 1 h can be observed when TEA was used as a scavenger. Contrary to this, rapid activation followed by slight deactivation in the similar overall reaction time (i.e., 1h) can be observed when TIBA was used in the reaction as a scavenger (compare **Figure 6** and **Figure 7**). In addition, higher one hour average activities (or productivities) were obtained when TIBA was used as scavenger, as shown in **Figure S10** of the supporting information. As discussed previously by Tisse et al.⁵¹, the lower activity observed in the presence of TEA can be ascribed to the formation of the hetero-bimetallic dormant species $[(n\text{Bu-Cp})_2\text{Zr}(\mu\text{R}_2)\text{AlR}_2]^+$ because the stability of the Zr/Al dormant species increases as the size of 'R' group decreases (i.e., size: Et < *i*-Bu).^{52,53} Moreover, the morphology of PE produced in all of these reactions was very similar showing spherical particles (**Figure S11**) and the bulk densities of the PE samples (presented in **Table 2**) also indicate that the polymerization occurred on the solid support.

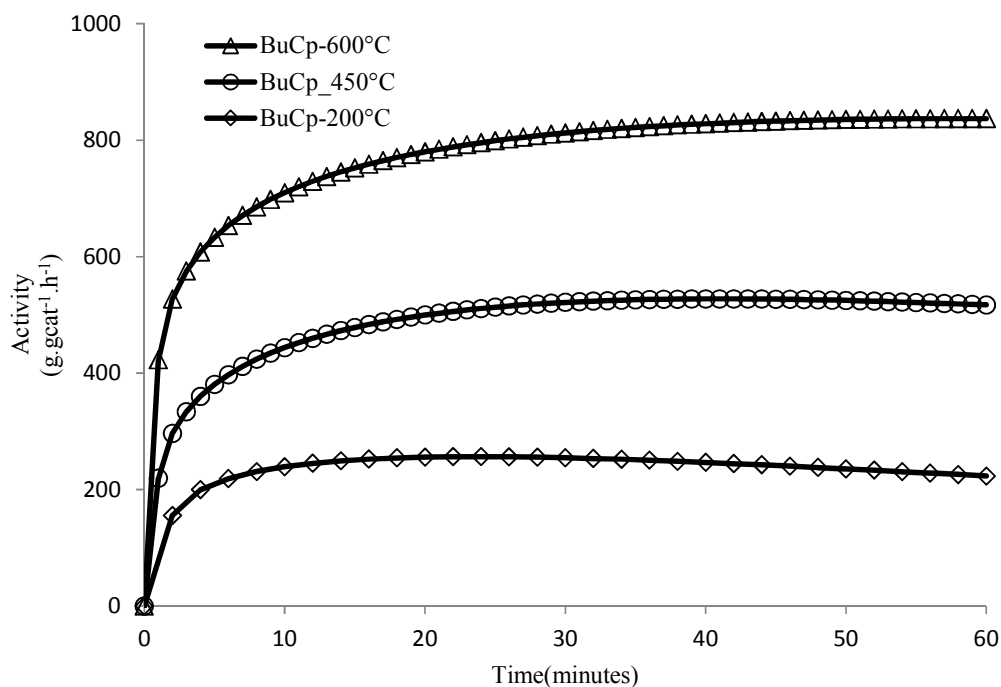


Figure 6. Comparison of slurry phase homopolymerization kinetic profiles of catalysts prepared with different silica dehydroxylation temperature using TEA as scavenger.

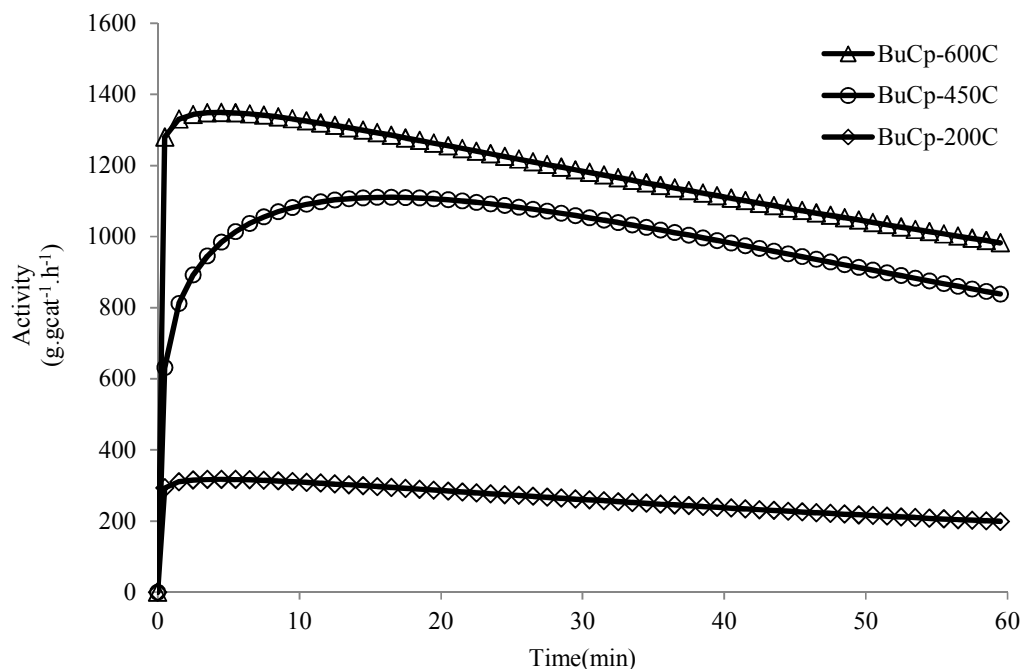


Figure 7. Comparison of slurry phase homopolymerization kinetic profiles of catalysts prepared with different silica dehydroxylation temperature using TIBA as scavenger.

Table 2. Comparison of catalytic activity and bulk densities of polymers produced in slurry and gas phase reactions.

Dehydroxylation Temperature (°C)	Al/Zr	Average Activity			Bulk Density	
		g gcat ⁻¹ h ⁻¹ (g gZr ⁻¹ h ⁻¹)			(g cm ⁻³)	
		Slurry TEA	Slurry TIBA	Gas TIBA	Slurry	Gas
200	499	227 ^a (2063) ^b	257 ^a (2336) ^b	223 ^a (2027) ^b	0.46	0.40
450	157	475 ^a (1637) ^b	981 ^a (3382) ^b	728 ^a (2510) ^b	0.34	0.32
600	148	855 ^a (3288) ^b	1162 ^a (4469) ^b	990 ^a (3807) ^b	0.38	0.34

For gas phase, polymerizations were run only using TIBA since no difference was observed in the molecular or physical properties of PE produced by using TEA in slurry polymerizations other than rise in intrinsic catalytic activity. The rate profiles of gas phase polymerizations, shown in **Figure 8**, have a different shape than the shape of slurry polymerization kinetic profiles with TIBA. In the gas phase, the initial rate rises more slowly to a maximum then the catalyst deactivates. Each catalyst reached its maximum activity in a different time. For example, the SMAO-200°C catalyst took 22 minutes, whereas, SMAO-600°C catalyst took 38 minutes to reach its maximum activity. A number of polymerizations were done to confirm these observations and the results are shown in **Figure S12** of the supporting information. It should be noted that the catalytic activity in g gcat⁻¹ h⁻¹ increased with increasing silica dehydroxylation temperature. Considering the wt% of Zr for the different catalysts it appears that the most efficient catalysts was the one obtained with SMAO-600°C. In addition, the final polymers showed similar molecular and physical characteristics, as shown in **Tables 3** of the next section, despite the different silica thermal treatments. This result is of high importance because it shows that the same active species are formed regardless the initial thermal treatment of silica, and that it appears that only the active site concentration changes.

The effect of silica thermal treatment on the performance of the catalyst studied here is twofold; i) it controls the percentage of co-catalytically active Aluminium species on SMAO leading to different concentrations of zirconocene in the final catalysts (i.e., lower zirconium content on catalyst prepared with SMAO-200°C than those prepared with SMAO-450°C or SMAO-600°C); and ii) it impacts the percentage of active Zr ($C^* = [Zr^*]/[Zr]$), since the highest catalytic activity was observed for n-BuCp-600°C catalyst (both in per g of catalyst and per mol of Zr).

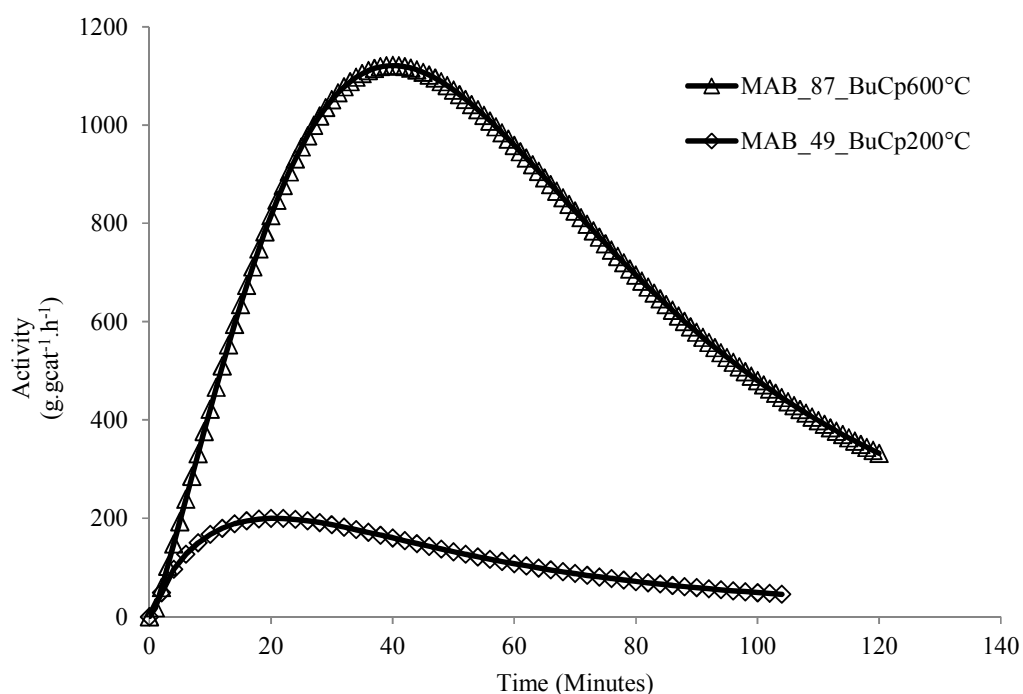


Figure 8. Comparison of gas phase homopolymerization kinetic profiles of catalysts prepared with different silica dehydroxylation temperature.

The difference of catalyst activation (as shown by the kinetic profiles) in slurry and gas phase polymerizations has also been observed by Kumkaew et al.,⁵⁴ who used $(nBuCp)_2ZrCl_2$

catalyst with similar Al/Zr molar ratios supported on similar silica supported and on mesoporous molecular sieves. Kumkaew et al.,⁵⁴ showed that the broadening of the kinetic profile in gas phase homo- and co-polymerizations with 1-hexene is related to the amount of triisobutyl aluminium (TIBA) and increased amounts of TIBA (e.g., 1 mmol) causes large induction periods (e.g., 40 min at 14 bar ethylene pressure), broadens the kinetic profile by increasing the time to reach maximum activity. On the other hand, slurry homopolymerization kinetic profiles with the same silica supported catalysts did not show induction period and were stable. It should be noted that in the present study, similar behaviour has been observed for both the slurry and gas phase ethylene homopolymerizations using the same catalyst. However, it is obvious from the **Figure 8** that no induction period was observed in the present work when using 1mmol TIBA in gas phase polymerizations.

In another work from the same group⁵⁵, effect of different alkylaluminium compounds including TIBA on gas phase ethylene homo and copolymerizations has been evaluated using $(n\text{-BuCp})_2\text{ZrCl}_2/\text{MAO}$ supported on polymeric supports. In the work of Hammawa et al.,⁵⁵ the kinetic profile obtained at highest TIBA reactor concentration i.e., 0.59 mmol in a 2 L reactor was very similar (i.e., in shape and time required to reach the maximum activity of $900 \text{ g gcat}^{-1} \text{ h}^{-1}$ approximately) to what is shown in Figure 8 for the catalyst prepared with SMAO-600°C. In the case of gas phase polymerization the initial local concentration of TIBA can be very high in the catalyst particles due to the low vapour pressure of this alkylaluminium which can certainly impact the initiation of the polymerization. Actually, a high local concentration of AlR_3 favours the formation of a dormant metallocenium-ion/TIBA complex in the initial stages of polymerization which is activated with time due to TIBA depletion. In case of slurry phase polymerization, the presence of diluent probably dilutes TIBA on catalyst active sites and therefore, activation of catalyst is fast.

Crystallinity and Molecular Masses of PE Samples

The average molecular weights, polydispersity (\bar{M}_w/\bar{M}_n) and crystallinity of the PE samples produced in slurry and gas phase polymerizations are shown in **Table 3**, and do not show any specific correlation with the silica dehydroxylation temperature. The polydispersity is close to the theoretical value of 2 for all samples, as expected of a single-site catalyst, thereby suggesting that the catalyst synthesis procedure does not lead to a multiplicity of active sites. In other words, the fact that the same polyethylene was produced regardless of the thermal treatment of silica and of the phase in which the reaction was performed tells us that the same active species were formed on the support. Thus, the dehydroxylation of silica appears to mainly impact the efficiency of the SMAO activator, i.e. the percentage of co-catalytically active aluminium site.

Table 3. MWD and crystallinity of slurry and gas phase PE samples.

Catalyst	Slurry Phase			Gas Phase		
	$M_w^a)$ g mol ⁻¹	$\bar{M}_w/\bar{M}_n^a)$	Crystallinity ^{b)} (%wt)	$M_w^a)$ g mol ⁻¹	$\bar{M}_w/\bar{M}_n^a)$	Crystallinity ^{b)} (%wt)
Cat-200°C	122100	2.2	65	143000	2.2	63
Cat-450°C	123600	2.3	66	119000	2.4	68
Cat-600°C	125600	2.2	63	127500	2.2	68

^{a)} Determined by high temperature SEC using triple detection. ^{b)} Determined by DSC

Conclusion

The concentration and the nature of silanol (Si-OH) groups on the surface of silica support is an important chemical property of silica, and significantly affects the catalytic activity of supported (n-BuCp)₂ZrCl₂ metallocene complex in ethylene homopolymerizations. Increasing the dehydroxylation temperature from 200°C to 600°C decreases the OH

concentration of silica and only isolated silanol groups remain on Grace 948 silica at 600°C. After impregnation of the silica with MAO the aluminium content of these silica (dehydroxylated at different temperatures) decreased with increase in dehydroxylation temperature. DRIFT and SS-NMR analyses showed that the grafting of MAO was impacted by the nature and the concentration of silanol groups on the silica surface. MAO reacted on silica dehydroxylated at high temperature (i.e., $\geq 450^\circ\text{C}$) with both silanol and siloxane groups which was evidenced by the formation of Si-Me. In addition, the presence of Al(Me)O₃ sites in different configuration was evidenced for the first time by SS-NMR in the present work. Consequently, the final supported metallocene catalysts showed a higher content of Zirconium at elevated dehydroxylation temperature (450-600°C). The intrinsic and average activity of (n-BuCp)₂ZrCl₂ supported on MAO impregnated silica (SMAO) in ethylene homopolymerizations was observed to increase with increasing silica dehydroxylation temperature from 200 to 600°C, both in slurry and gas phase processes. Furthermore, no significant effect of silica dehydroxylation temperature was observed on the MWD and crystallinity of the polyethylene produced both in slurry and gas phase polymerizations. Thus, whatever the thermal treatment of silica is, the same active species are formed but more active sites are generated when silica was thermally treated at high temperature.

Acknowledgment

Financial support by the Dutch Polymer Institute is gratefully acknowledged. This work is a part of the Research Programme of the Dutch Polymer Institute (DPI, Eindhoven, The Netherlands), Project no. 753. The authors are also thankful to Dr. John Severn of DSM Ahead, Geleen, The Netherlands for providing assistance in the synthesis of catalysts.

Electronic Supporting Information

Silica dehydroxylation profiles, DRIFT spectra of silica-200°C, SMAO-200°C, n-BuCp/SMAO-200°C, silica-450°C, SMAO-450°C, n-BuCp/SMAO-450°C, ^1H proton NMR of undried and dried MAO, ^1H MAS NMR spectrum of AlMe_3 grafted on $\text{SiO}_2\text{-600}$, ^{27}Al MQ MAS spectrum of MAO, ^{27}Al MQ MAS isotropic projections of dried MAO (top) and SMAO-600, Average activities (or productivity) of the catalysts with different silica dehydroxylation temperatures, Comparison of polyethylene morphology produced in slurry and gas phase polymerizations, Comparison and reproducibility of catalysts average activity (or productivity) in gas phase homopolymerizations.

Notes and References

1. J.R. Severn. In *Tailor-Made Polymers*, Eds. J.R. Severn, J.C. Chadwick., Wiley-VCH Verlag GmbH & Co. KGaA, Weinheim, 2008. pp 98-138
2. F. Ghiotto, C. Pateraki, J. Tanskanen, J.R. Severn, N. Luehmann, A. Kusmin, J. Stellbrink, M. Linnolahti, M. Bochmann, *Organometallics.*, 2013, **32**, 3354-3362.
3. J.T. Hirvi, M. Bochmann, J.R. Severn, M. Linnolahti, *ChemPhysChem.*, 2014, **15**, 2732-2742.
4. D. Bianchini, J.H.Z. dos Santos, T. Uozumi, T. Sano, *J. Mole. Catal. A- Chemical.*, 2002, **185**, 223-235.
5. V.N. Panchenko, N.V. Semikolenova, I.G. Danilova, E.A. Paukshtis, V.A. Zakharov, *J. Mole. Catal. A- Chemical.*, 1999, **142**, 27-37.
6. J.H.Z. dos Santos, C. Krug, M.B. da Rosa, F.C. Stedile, J. Dupont, M. de Camargo Forte, *J. Mole. Catal. A- Chemical.*, 1999, **139**, 199-207.
7. D. Bianchini, F.C. Stedile, J.H.Z. dos Santos, *App. Catal. A- General.*, 2004, **261**, 57-67.
8. M. Atiqullah, M.N. Akhtar, A.A. Moman, A.H. Abu-Raqabah, S.J. Palackal, H.A. Al-Muallem, O.M. Hamed, *App. Catal. A- General.*, 2007, **320**, 134-143.
9. M.J.D. Low, A.G. Severdia, J. Chan, *J. Catal.*, 1981, **69**, 384-391.
10. R. van Grieken, A. Carrero, I. Suarez, B. Paredes, *Euro. Polym. J.*, 2007, **43**, 1267-1277.

11. B. Kou, K.B. McAuley, C.C. Hsu, D.W. Bacon, K.Z. Yao, *Ind. Eng. Chem. Res.*, 2005, **44**, 2443-2450.
12. B. Paredes, R.v. Grieken, A. Carrero, I. Suarez, J.B.P. Soares, *Macromol. Chem. Phys.*, 2011, **212**, 1590-1599.
13. J.M. Zhou, N.H. Li, N.Y. Bu, D.T. Lynch, S.E. Wanke, *J. Appl. Polym. Sci.*, 2003, **90**, 1319-1330.
14. G.G. Hlatky, *Chem. Rev.*, 2000, **100**, 1347-1376.
15. *US Pat.*, 6469113 B1., 1999.
16. M. Smit, X. Zheng, J. Loos, J.C. Chadwick, C.E. Koning, *J. Polym. Sci. A Polym. Chem.*, 2005, **43**, 2734-2748.
17. M. Namkajorn, A. Alizadeh, E. Somsook, T.F.L. McKenna, *Macromol. Chem. Phys.*, 2014, **215**, 873-878.
18. A. Brinkmann, A.P.M. Kentgens, *J. Am. Chem. Soc.*, 2006, **128**, 14758-14759.
19. M. Carravetta, M. Eden, X. Zhao, A. Brinkmann, M.H. Levitt, *Chem. Phys. Lett.*, 2000, **321**, 205-215.
20. J.P. Amoureux, C. Fernandez, S. Steuernagel, *J. Magn. Reson. Ser- A.*, 1996, **123**, 116-118.
21. B. Wunderlich. *Thermal Analysis*, Academic Press Inc, San Diego, 1990.
22. J.R. Severn, J.C. Chadwick., *Tailor-Made Polymers: Via Immobilization of Alpha-Olefin Polymerization Catalysts*, Wiley-VCH Verlag GmbH & Co. KGaA, Weinheim, 2008.
23. J.R. Severn, J.C. Chadwick, R. Duchateau, N. Friederichs, *Chem. Rev.*, 2005, **105**, 4073-4147.
24. D.W. Imhoff, L.S. Simeral, S.A. Sangokoya, J.H. Peel, *Organometallics.*, 1998, **17**, 1941-1945.
25. M. Jezequel, V. Dufaud, M.J. Ruiz-Garcia, F. Carrillo-Hermosilla, U. Neugebauer, G.P. Niccolai, F. Lefebvre, F. Bayard, J. Corker, S. Fiddy, J. Evans, J.P. Broyer, J. Malinge, J.M. Basset, *J. Am. Chem. Soc.*, 2001, **123**, 3520-3540.
26. V.N. Panchenko, L.G. Echevkaya, V.A. Zakharov, M.A. Matsko, *App. Catal. A-General.*, 2011, **404**, 47-53.
27. I. Tritto, C. Mealares, M.C. Sacchi, P. Locatelli, *Macromol. Chem. Phys.*, 1997, **198**, 3963-3977.
28. L. Britcher, H. Rahiala, K. Hakala, P. Mikkola, J.B. Rosenholm, *Chem. Mater.*, 2004, **16**, 5713-5720.

29. D.E. Babushkin, N.V. Semikolenova, V.N. Panchenko, A.P. Sobolev, V.A. Zakharov, E.P. Talsi, *Macromol. Chem. Phys.*, 1997, **198**, 3845-3854.
30. M.R. Mason, J.M. Smith, S.G. Bott, A.R. Barron, *J. Am. Chem. Soc.*, 1993, **115**, 4971-4984.
31. C.J. Harlan, M.R. Mason, A.R. Barron, *Organometallics.*, 1994, **13**, 2957-2969.
32. R. Benn, A. Rufinska, H. Lehmkuhl, E. Janssen, C. Kruger, *Angew. Chem. Int. Ed. Engl.*, 1983, **22**, 779-780.
33. R. Benn, E. Janssen, H. Lehmkuhl, A. Rufinska, *J. Organomet. Chem.*, 1987, **333**, 155-168.
34. P.L. Bryant, C.R. Harwell, A.A. Mrse, E.F. Emery, Z. Gan, T. Caldwell, A.P. Reyes, P. Kuhns, D.W. Hoyt, L.S. Simeral, R.W. Hall, L.G. Butler, *J. Am. Chem. Soc.*, 2001, **123**, 12009-12017.
35. F.J. Wu, L.S. Simeral, A.A. Mrse, J.L. Eilertsen, L. Negureanu, Z. Gan, F.R. Fronczek, R.W. Hall, L.G. Butler, *Inorg. Chem.*, 2007, **46**, 44-47.
36. I. Schnell, S.P. Brown, H.Y. Low, H. Ishida, H.W. Spiess, *J. Am. Chem. Soc.*, 1998, **120**, 11784-11795.
37. R. Anwander, C. Palm, O. Groeger, G. Engelhardt, *Organometallics.*, 1998, **17**, 2027-2036.
38. J. Li, J.A. DiVerdi, G.E. Maciel, *J. Am. Chem. Soc.*, 2006, **128**, 17093-17101.
39. J. Trebosc, B. Hu, J.P. Amoureux, Z. Gan, *J. Magn. Reson.*, 2007, **186**, 220-227.
40. L. Frydman, J.S. Harwood, *J. Am. Chem. Soc.*, 1995, **117**, 5367-5368.
41. I. Hung, J. Trebosc, G.L. Hoatson, R.L. Vold, J.P. Amoureux, Z. Gan, *J. Magn. Reson.*, 2009, **201**, 81-86.
42. X. Wang, J. Adhikari, L.J. Smith, *J. Phys. Chem. C.*, 2009, **113**, 17548-17559.
43. M.P. J.P. Amoureux. In *Encyclopedia of Nuclear Magnetic Resonance*, Eds. R.K.H. D.M. Grant., John Wiley, Chichester, 2002; Vol. 9.
44. S.J. Obrey, S.G. Bott, A.R. Barron, *Organometallics.*, 2001, **20**, 5119-5124.
45. E. Mazoyer, J. Trebosc, A. Baudouin, O. Boyron, J. Pelletier, J.M. Basset, M.J. Vitorino, C.P. Nicholas, R.M. Gauvin, M. Taoufik, L. Delevoye, *Angew. Chem. Int. Edit.*, 2010, **49**, 9854-9858.
46. Z. Boudene, T. De Bruin, H. Toulhoat, P. Raybaud, *Organometallics.*, 2012, **31**, 8312-8322.

47. K. Mackenzie, M. Smith. In *Pergamon Materials Series Multinuclear Solid-State NMR of Inorganic Materials*, Volume 6 ed.; Eds. J.D.M. Kenneth., Pergamon, 2002.
48. R.N. Kerber, A. Kermagoret, E. Callens, P. Florian, D. Massiot, A. Lesage, C. Coperet, F. Delbecq, X. Rozanska, P. Sautet, *J. Am. Chem. Soc.*, 2012, **134**, 6767-6775.
49. R. Benn, E. Janssen, H. Lehmkuhl, A. Rufinska, *J. Organo. Chem.*, 1987, **333**, 169-180.
50. H.S. Zijlstra, S. Harder, *Eur. J. Inorg. Chem.*, 2015, **2015**, 2.
51. V.F. Tisse, C. Boisson, T.F.L. McKenna, *Macromol. Chem. Phys.*, 2014, **215**, 1358-1369.
52. M. Bochmann, S.J. Lancaster, *Angew. Chem. Int. Ed. Engl.*, 1994, **33**, 1634-1637.
53. F. Song, R.D. Cannon, M. Bochmann, *J. Am. Chem. Soc.*, 2003, **125**, 7641-7653.
54. P. Kumkaew, S.E. Wanke, P. Prasertdam, C. Danumah, S. Kaliaguine, *J. Appl. Polym. Sci.*, 2003, **87**, 1161-1177.
55. H. Hammawa, T.M. Mannan, D.T. Lynch, S.E. Wanke, *J. Appl. Polym. Sci.*, 2004, **92**, 3549-3560.

Table of Content/Graphical Abstract

